Desalination and Water Treatment
www.deswater.com
doi: 10.5004/dwt.2021.27455

232 (2021) 39–54
August

Optimization of ammonium adsorption from landfill leachate using montmorillonite/hematite nanocomposite: response surface method based on central composite design

Hassan Hashemi[a], Shima Bahrami[a], Zahra Emadi[b], Hamideh Shariatipor[a], Majid Nozari[c,*]

[a]*Research Center for Health Sciences, Shiraz University of Medical Sciences, Shiraz, Iran, emails: h_hashemi@sums.ac.ir (H. Hashemi), bahramishima31@gmail.com (S. Bahrami), Hamideh.shariaty@gmail.com (H. Shariatipor)*
[b]*Department of Environmental Health, School of Public Health, Shahrekord University of Medical Sciences, Shahrekord, Iran, email: Zahra.emadi1987@yahoo.com*
[c]*Department of Environmental Health Engineering, Faculty of Public Health, Kerman University of Medical Sciences, Kerman, Iran, Tel. +98-9383921819; email: nozari.m@kmu.ac.ir*

Received 26 December 2020; Accepted 18 May 2021

ABSTRACT

In this study, the adsorption of ammonium ions from landfill leachate (LL) was examined using montmorillonite/hematite nanocomposite (M/HNC). Parameters affecting ammonium adsorption such as pH 3–11, adsorbent dosage 0.05–0.25 g/L, mixing speed 75–175 rpm, and contact time 25–125 min were assessed. The central composite design (CCD)–based response surface methodology was employed to design the experiments and find optimal conditions. M/HNC was synthesized under green conditions and structurally investigated using X-ray powder diffraction, Fourier-transform infrared spectroscopy, Brunauer–Emmett–Teller, and scanning electron microscopy techniques. M/HNC was synthesized with a particle size of about 26 nm, magnetic properties, and a high specific surface area. The efficiency of ammonium adsorption from LL was increased by enhancing parameters such as pH, adsorbent dosage, mixing speed, and contact time. The pH of 8.05, adsorbent dosage of 0.167 g/L, mixing speed of 117.42 rpm, and contact time of 81.99 min was presented as optimal conditions according to the results of the CCD method. In addition, the efficiency of ammonium adsorption from LL using M/HNC was 80% at optimal conditions. The data of ammonium adsorption on M/HNC fitted well with pseudo-second-order kinetic and Langmuir isotherm models. It should be noted that the interactive effects of the parameters had an increasing impact on the ammonium adsorption efficiency. Based on the results of the present study, M/HNC had an effective potential for the adsorption of ammonium from LL.

Keywords: Ammonium; Landfill leachate; Montmorillonite/hematite nanocomposite; Central composite design

1. Introduction

Wastes are recognized as a threat to human survival, living organisms, and natural resources that are necessary for human life [1]. In fact, poor waste management can cause soil, water, and atmospheric pollution [2]. Moreover, urban solid waste can block drains, accumulate stagnant water which spreads insects, and cause floods during the rainy seasons [3].

Precipitation, rainfall, and water flow from solid waste can cause the production of heavy wastewater, which is known as landfill leachate (LL) [4–6]. Depending on the type and density of wastes, age and hydrology of landfill, and climate, LL includes different substances such as heavy

* Corresponding author.

metals, ammonia, organic matters, and other hazardous materials [7–9].

The presence of ammonium in the aquatic environment results in the reduction of dissolved oxygen and eutrophication and can also be toxic for fish and humans [10–12]. Due to the adverse effects of ammonium, it should be removed from the environment.

Air stripping, nitrification/denitrification, and chemical precipitation are the traditional treatment systems used for the removal of ammonium from wastewater [13]. Biological nitrification/denitrification is the most common and effective method for ammonium removal. However, the bio-transformation of ammonium is slow and special temperature and climate situations are necessary for this method. Air stripping is a simple method that is not sensitive to toxic compounds. High aeration rate, temperatures more than 15°C, and pH > 9.5 are the most important reasons that lead to an increase in cost [14,15]. However, methods such as adsorption and ion exchange are more efficient and cost-beneficial. Moreover, these methods may be less affected by fluctuations in wastewater quality and temperature [16]. Adsorption is a process that can transfer the adsorbate in the liquid phase to the surface of the adsorbent solid phase [17]. Natural clays are very popular and practical for the adsorption of ammonium from the environment due to their cheapness, accessibility, and ease of application [18].

Montmorillonite is a 2:1 clay with an octahedral aluminum sheet (Al^{3+}) that is interlayered between two tetrahedral silica sheets (Si^{4+}) [19]. High cation exchange capacity and specific surface area, mechanical and chemical stableness, and layered construction are some of the characteristics of montmorillonite [20]. Therefore, montmorillonite has been applied as an adsorbent for the adsorption of cationic pollutants. Adsorption of Pb^{2+}, Ni^{2+}, Cd^{2+}, Cu^{2+}, and Zn^{2+} using montmorillonite has been reported in different studies [21–23]. Direct reduction of iron (Midrex) is a process in which iron ore is reduced and then a sponge is created [24]. Different forms of iron (hematite, magnetite, and wüstite) are produced in the reduction process and can be applied as industrial wastes for the modification of clays instead of different commercial chemicals and wastes such as agricultural wastes [25].

Adsorption of ammonium from synthetic wastewater by different clays has been investigated in previous studies [26,27]. However, few studies have focused on the adsorption of ammonium from real wastewater, especially LL [28,29]. In most studies, commercial iron oxides were used in combination with montmorillonite clay as an adsorbent in order to eliminate ammonium [30,31]. In this study, hematite (a type of industrial waste obtained from the Midrex process) along with montmorillonite was used as a cheap and available adsorbent, which can be a suitable solution for waste management in steel industries and waste reuse. Therefore, the present study aimed to investigate the efficiency of ammonium ion adsorption from LL by montmorillonite/hematite nanocomposite (M/HNC). The effect of different parameters such as pH, adsorbent dosage, mixing speed, and contact time on the ammonium adsorption efficiency was investigated using response surface methodology (RSM) based on central composite design (CCD).

2. Material and methods

2.1. Source of LL

LL was collected from the BarMe Shor waste site (16 km east of Shiraz) in Fars Province, Iran. The area of the site is 5,000 ha, 40 ha of which is used for landfilling. The sample was stored in a box with ice packs and carried to the laboratory. Then, it was kept in a refrigerator at 4°C to prevent the biodegradation of LL. The characteristics of LL after dilution with deionized water (1:5) are shown in Table 1.

2.2. Chemicals

Montmorillonite ($MgNaAl_5(Si_4O_{10})_3(OH)_6$) was purchased from Sigma-Aldrich (USA, CAS Number 1318–93–0). Ammonium hydroxide, hydrochloric acid, sodium hydroxide, and ethanol were purchased from Merck (Germany). Alkaline cyanide, polyvinyl alcohol (dispersing agent), and mineral stabilizer were purchased from HACH (USA).

2.3. Synthesis of the adsorbent

First, montmorillonite was washed three times with deionized water and dried at 120°C for 10 h [18]. After that, dried clay was powdered and sieved. In the present study, instead of high purity iron, industrial waste containing iron was applied for the modification of montmorillonite. The waste was prepared from the furnaces of the Midrex process in a steel factory in Fars Province, Iran. In the second step, M/HNC was synthesized according to the method described by Lassoued et al. [32] with a slight modification. In brief, 100 mL of deionized water was added to 2 g of the iron compound and stirred. Then 2 g of sieved montmorillonite was added and the solution was stirred again. During the stirring, an ammonia solution (2 M, NH_4OH) was added to the above solution until the pH reached 11 at 80°C, and then the solution was shaken for 4 h. In the last step, the solution was cooled off (room temperature) and filtered. The precipitate was washed with deionized water and ethanol and dried at 80°C. M/HNC was kept in a desiccator until use in the experiments.

2.4. Specifications of the adsorbent

The crystalline structure of M/HNC was analyzed by X-ray powder diffraction (XRD). XRD measurement was

Table 1
Characteristics of LL

Parameters	Value
NH_4^+ (mg/L)	30
pH	4.5
COD (mg/L)	18,000
BOD_5 (mg/L)	10,000
TSS (mg/L)	500
TOC (mg/L)	6,000

COD: Chemical oxygen demand; BOD: Biochemical oxygen demand; TSS: Total suspended solids; TOC: Total organic carbon

carried out by PANalytical X'Pert Pro using Cu Kα radiation over a 2θ range of 5°–100°. Functional groups were detected by the Fourier-transform infrared spectroscopy (FTIR) analysis using KBr powder in the range of 400–4,000 cm^{-1} for montmorillonite and M/HNC (Thermos Avatar, USA). The surface morphology and particle size of montmorillonite and M/HNC (before and after the adsorption of ammonium) were investigated by scanning electron microscopes (SEM) MIRA3 TESCAN. The Brunauer–Emmett–Teller (BET) surface area and pore size of M/HNC were also investigated using N_2 adsorption–desorption isotherms via the Belsorp-mini II (Japan) model analysis.

2.5. Batch adsorption tests

Adsorption experiments were performed in 250 mL Erlenmeyer flasks in the final volume of 100 mL. The effect of different levels of operational variables such as pH 3, 5, 7, 9, and 11, adsorbent dosage 0.05, 0.1, 0.15, 0.2, and 0.25 g/L, mixing speed 75, 100, 125, 150, and 175 rpm, and contact time 25, 50, 75, 100, and 125 min on the adsorption efficiency of ammonium was studied by the CCD method. HCl and NaOH (1 N) were used for adjusting pH. After performing the adsorption experiments, the samples were drawn and centrifuged at 4,500 rpm for 15 min. The residual concentration of ammonium in the samples was analyzed according to the Nessler method, and the absorbance of each sample (after adding the reagents) at 425 nm was determined by a UV-Vis spectrophotometer (DR5000, HACH, USA). Finally, the adsorption efficiency of ammonium was calculated using Eq. (1):

$$\text{Adsorption efficiency}(\%) = \frac{C_i - C_f}{C_i} \times 100 \quad (1)$$

where C_i and C_f are the initial and final concentrations of ammonium, respectively. All the experiments were done in triplicate.

Moreover, the adsorption capacity of M/HNC was determined by Eq. (2) [33,34]:

$$q_e(\text{mg/g}) = \frac{(C_0 - C_e)V}{M} \quad (2)$$

where q_e, C_0, C_e, V, and M are the adsorption capacity of M/HNC (mg/g), initial concentration of ammonium (mg/L), equivalent concentration of ammonium (mg/L), volume of the solution (L), and dosage of M/HNC (g), respectively.

2.6. Method of analysis

RSM is considered a great tool for reducing the number of experiments and saving time compared with the single-factor optimization method. Also, RSM can be applied as a statistical tool for determining the main and interactive effects of the variables [35–39]. Clearly, the CCD model also has its limitations, which include the following: (i) it was observed that the star points are outside the hypercube, so the number of levels that have to be adjusted for every factor is five instead of three, and sometimes it is not easy to achieve the adjusted values of factors. (ii) Depending on the design, the squared terms in the model will not be orthogonal to each other. (iii) Individual interaction terms, that is, linear by quadratic or quadratic by quadratic cannot be estimated [40]. In this study, RSM based on CCD was used as an experimental design model to evaluate the optimum conditions of ammonium adsorption. Thirty runs involving four factors (pH, adsorbent dosage, mixing speed, and contact time) were designed for the experiments using Design-Expert 11 (Table 2). It should be noted that statistical significance ($p \le 0.05$) was analyzed with an *F*-test via the analysis of variance (ANOVA). Finally, the interactive effects of the variables on the adsorption of ammonium were represented by three-dimensional diagrams (3D). The CCD involves 2^K factorial runs, 2*K* axial runs, and *C* center runs. The CCD design comprises five coded levels of –α, −1, 0, +1, and +α, corresponding to the lower axial, low, medium, high, and upper axial points, respectively. The α value is calculated by $\alpha = 2^{k/4}$ in which *k* indicates the number of factors; in this study, this value was specified to be 2. The total number of experiments (*N*) is defined by Eq. (4), and in this circumstance, the number is 30 for $k = 4$ (four variables investigated). The optimization of the experiments was determined by analyzing the response for ammonium adsorption. The response function as a second-order polynomial was determined by using regression analysis. The quadratic model is as follows [Eq. (3)]:

$$Y = \beta_0 + \sum \beta_i X_j + \sum \beta_{ij} X_i X_j + \sum \beta_{ii} X_i^2 \quad (3)$$

$$N = 2^K + 2K + C \quad (4)$$

where *Y*: ammonium adsorption efficiency, X_i and X_j: independent variables, β_0: constant coefficient, β_i: linear order interaction, β_{ij}: second-order interaction, and β_{ii}: quadratic coefficients. Also, *K* is the number of independent variables (factors), *C* is the number of center points, and *N* is the overall total of experimental runs [40].

Table 2
The levels and codes of variables for the ammonium adsorption process

Factor	Name	Units	Minimum (–α)	Low (–1)	Center (0)	High (+1)	Maximum (+α)
A	pH	–	3	5	7	9	11
B	Adsorbent dosage	g/L	0.05	0.1	0.15	0.2	0.25
C	Mixing speed	rpm	75	100	125	150	175
D	Contact time	min	25	50	100	75	125

2.7. Determination of pH_{pzc}

To determine the pH_{pzc} (point of zero charge) of M/HNC, 50 mL of 0.1 M NaCl was added to eleven 100 mL Erlenmeyer flasks. The initial pH in all the flasks was adjusted by 1 M HCL and NaOH in the range of 1 to 11. Then, 0.05 g of M/HNC was added to all the flasks and stirred by a shaker at 120 rpm for 48 h. The adsorbent was separated by a neodymium magnet after 48 h and the pH was remeasured in all the flasks and recorded as the final pH. Finally, a diagram of the initial pH vs. ΔpH (pH_{final} – $pH_{initial}$) was plotted and the pH_{pzc} value was reported [34,41,42].

2.8. Adsorption kinetics study

Adsorption kinetics of ammonium with M/HNC at the initial concentration of 30 mg/L, contact time of 0–115 min, adsorbent dose of 0.167 g/L, pH = 8.05, mixing speed of 117.42 rpm, and temperature of 25°C was investigated. The two kinetic models were applied for the determination of the reaction order. Pseudo-first-order and pseudo-second-order models were estimated by Eqs. (5) and (6).

$$\log\left(q_e - q_t\right) = \log q_e - k_1 t \tag{5}$$

$$\frac{t}{q_t} = \frac{1}{k_2 q_e^2} + \frac{1}{q_e} t \tag{6}$$

where q_e, q_t, t, k_1, and k_2 are the adsorption capacity of M/HNC at equilibrium (mg/g), adsorption capacity of M/HNC at time t (mg/g), time (min), pseudo-first-order constant (1/min), and pseudo-second-order constant (g/mg min), respectively [33,43,44].

2.9. Adsorption isotherm study

The isotherm of ammonium adsorption was investigated by Langmuir and Freundlich models. The ammonium adsorption isotherms demonstrated the relationship between the amount of ammonium adsorbed and the equilibrium ammonium concentration at a constant temperature. Isothermal experiments of ammonium adsorption on M/HNC at initial concentrations of 5–30 mg/L, contact time of 0–115 min, adsorbent dose of 0.167 g/L, pH = 8.05, mixing speed of 117.42 rpm, and temperature of 25°C were investigated. Eqs. (7) and (8) were applied for determining the Langmuir and Freundlich isotherms:

$$\frac{C_e}{q_e} = \frac{1}{q_{\max}} + \frac{K_L + C_e}{q_{\max}} \tag{7}$$

$$\log q_e = \log K_F + \frac{\log C_e}{n} \tag{8}$$

where C_e, q_e, q_{max}, K_L, K_F, and n are the equilibrium ammonium concentration (mg/L), equilibrium amount of ammonium adsorbed by M/HNC (mg/g), maximum adsorption of ammonium (mg/g), Langmuir constant (L/mg), Freundlich constant ((mg/g) (mg/L)^n), and adsorption intensity, respectively [33,34].

3. Results and discussion

3.1. Specifications of M/HNC

3.1.1. Scanning electron microscopy

The morphology and structure of the samples were identified by SEM. As shown in Fig. 1a, montmorillonite has a layered structure, which was in agreement with the

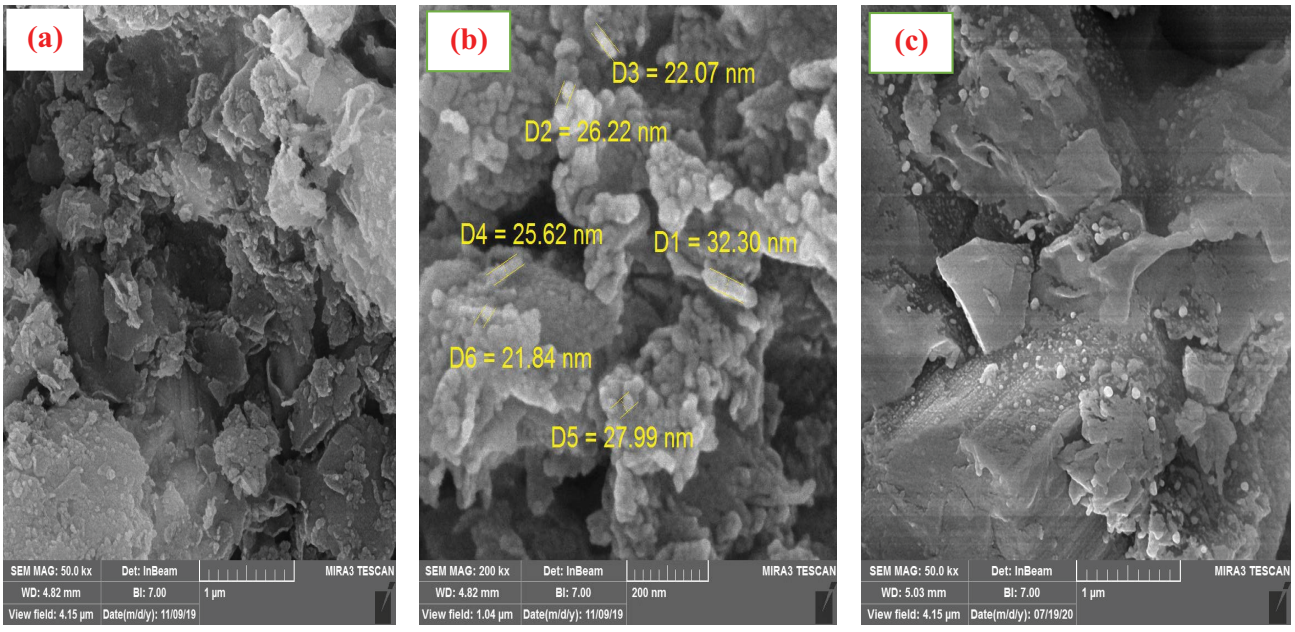

Fig. 1. SEM image of (a) montmorillonite, (b) M/HNC before the adsorption process, and (c) M/HNC after the adsorption process.

results of the study by Zheng et al. [30]. It can be observed that M/HNC has a spherical shape within the size range of 15–40 nm [45] which confirms that this adsorbent has a nanostructure (Fig. 1b). Moreover, the change in the surface of M/HNC might be due to the adsorption of various pollutants such as the ammonium in LL on the adsorbent (Fig. 1c).

3.1.2. Fourier-transform infrared spectroscopy

The FTIR spectra of montmorillonite and M/HNC are shown in Fig. 2. The peaks at 3,450.79 and 3,629.01 cm^{-1} (montmorillonite) and 3;437.07; 3,749.21 and 2,925.88 cm^{-1} (M/HNC) were due to the OH stretching of interlayer water and the hydroxyl groups [46–48]. The increase in the number of hydroxyl peaks in M/HNC could be due to the consumption of ammonium hydroxide, water, and ethanol for the synthesis of the adsorbent. The peaks in the region of 600–1300 cm^{-1} were related to Si–O in montmorillonite and M/HNC [47,48]. The peaks at 469.95 and 546.69 cm^{-1} could be attributed to the Fe–O band vibration in M/HNC, which was not present in montmorillonite [32]. It should be noted that the peak at 522.44 cm^{-1} in montmorillonite might be due to the presence of Si–O–Al [49].

3.1.3. Brunauer–Emmett–Teller

The synthesized M/HNC BET specific surface area and adsorption/desorption isotherm are shown in Fig. 3. The synthesized M/HNC specific surface area, mean pore diameter, and total pore volume (p/p_0 = 0.99) were obtained to be 102.16 m^2/g, 7.7325 nm, and 0.2152 cm^3/g, respectively. According to the IUPAC, pores are arranged into three groups: Microporous, mesoporous, and macroporous materials [50]. Based on the IUPAC definition, a mesoporous material contains pores with diameters between 2 and 50 nm. Moreover, the pore sizes of microporous and macroporous materials are smaller than 2 nm and larger

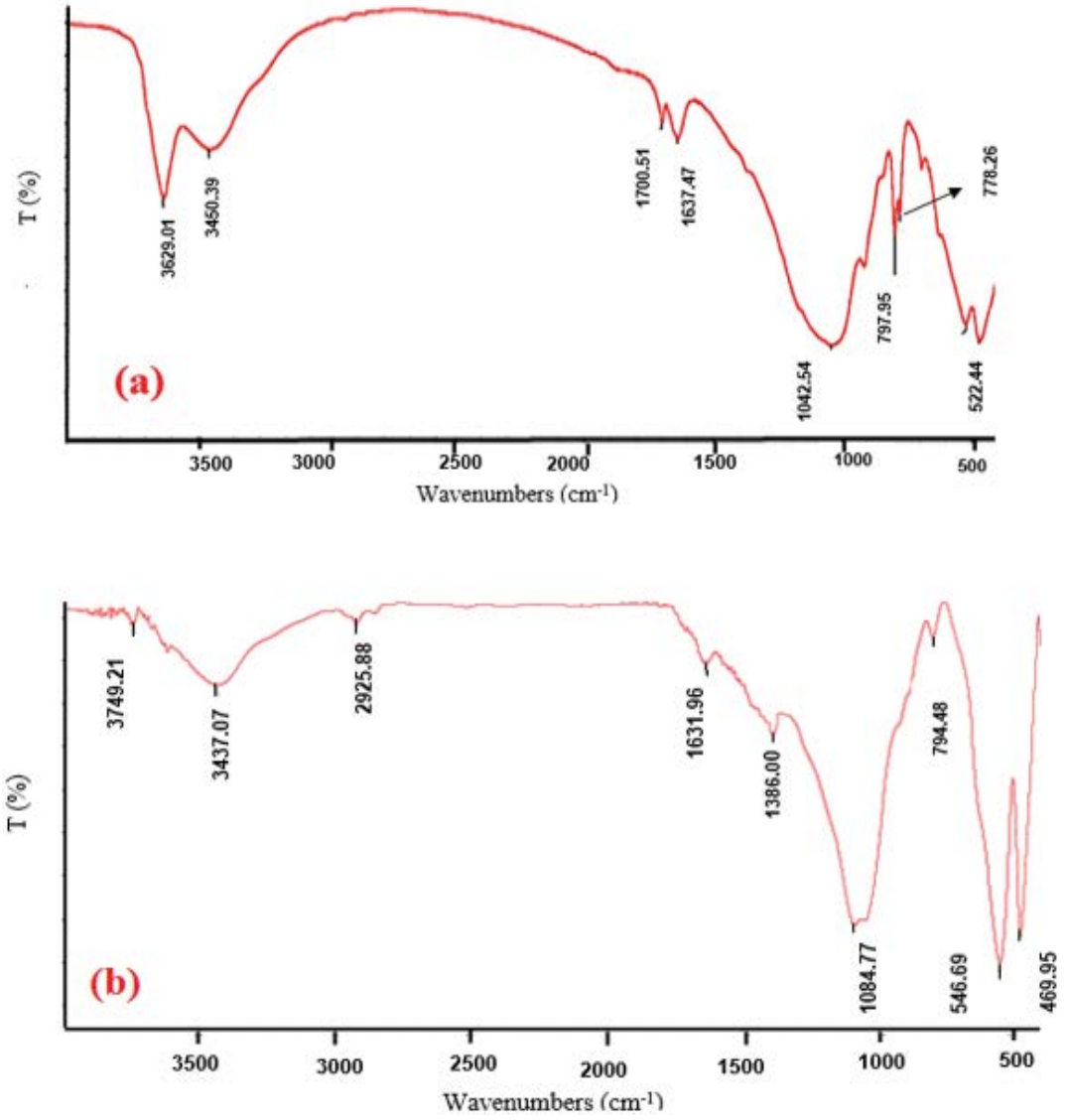

Fig. 2. FTIR spectra of (a) montmorillonite and (b) M/HNC.

than 50 nm, respectively. M/HNC could be classified as a mesoporous material.

3.1.4. X-ray powder diffraction

The XRD pattern of M/HNC is shown in Fig. 4. The peaks at 24.22, 33.22, 35.68, 40.91, 43.36, 49.51, 54.11, 57.65, 62.48, 64.05, 69.75, and 75.51 indicated the formation and presence of hematite. Fouad et al. [48] and Wahab et al. [51] reported the same peaks for hematite. The peaks at 21.93, 26.68, and 29.47 showed the presence of montmorillonite in the adsorbent [30,52]. Also, the peaks at 68.20 and 68.40 indicated that montmorillonite has a dioctahedral structure [49].

3.2. Statistical analysis and determining the mathematical correlation between the variables and ammonium adsorption efficiency

Ammonium adsorption efficiencies under the determined conditions are shown in Table 3. Based on the results, the adsorption of ammonium ranged from 47.22% to 90.04%, and the maximum adsorption efficiency occurred at pH = 11, 0.15 g/L of M/HNC, 125 rpm, and 75 min (run = 8). The adsorption capacity of the adsorbent was in the range of 90.18–376.92 mg/g, which demonstrated a considerable adsorption capacity for the present adsorbent.

The relationship between the predicted and observed (actual) ammonium adsorption values was investigated by

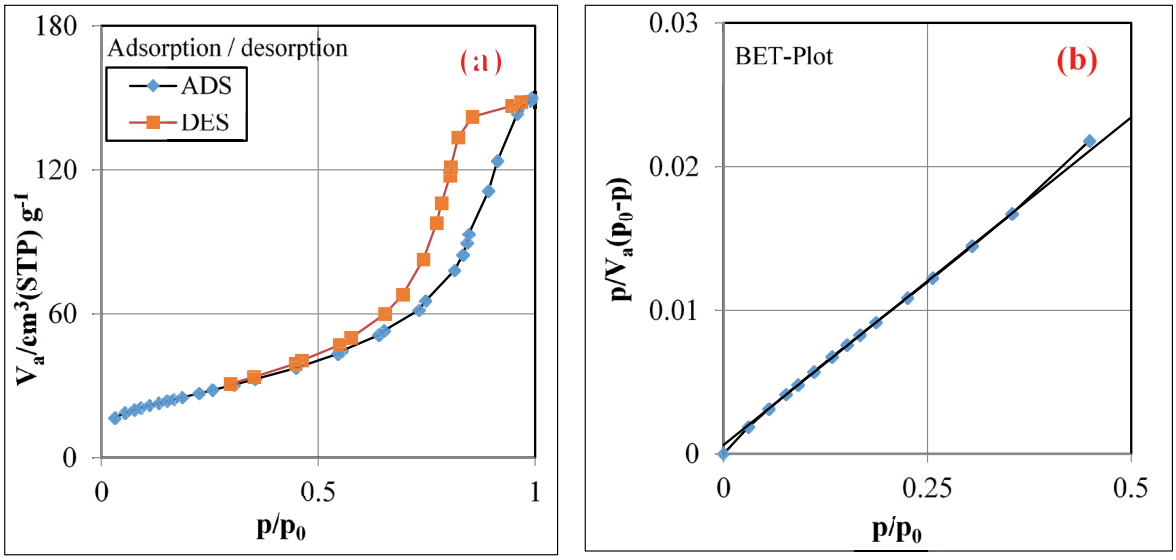

Fig. 3. (a) Adsorption/desorption isotherm and (b) BET surface area of M/HNC.

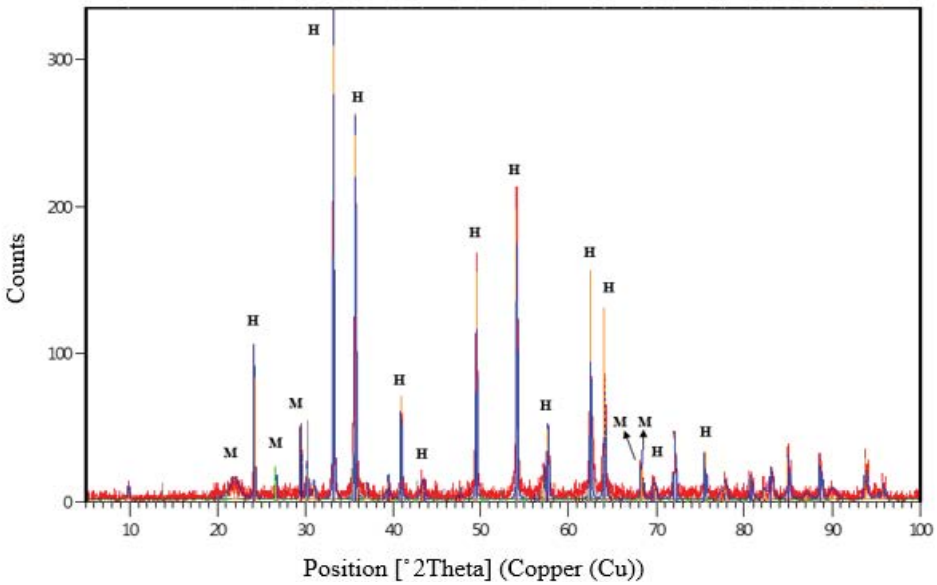

Fig. 4. XRD pattern of M/HNC (M: Montmorillonite, H: Hematite).

Table 3
CCD matrix for the ammonium adsorption process

Run	*A*: pH (–)	*B*: adsorbent dosage (g/L)	*C*: mixing speed (rpm)	*D*: contact time (min)	Adsorption efficiency (%)		Adsorption capacity (mg/g)
					Predicted	Actual	
1	5	0.1	150	100	58.22	57.12	171.36
2	9	0.2	150	100	87.17	86.42	129.63
3	7	0.15	75	75	72.67	73.54	147.08
4	9	0.2	100	100	86.02	85.04	127.76
5	5	0.2	150	100	65.35	64.04	96.06
6	7	0.15	125	25	70.27	71.15	142.30
7	5	0.1	150	50	56.25	56.19	168.57
8	11	0.15	125	75	89.76	90.04	180.08
9	7	0.15	125	75	74.63	75.38	150.76
10	7	0.15	125	75	74.63	74.31	148.62
11	9	0.1	150	50	78.77	79.67	239.01
12	3	0.15	125	75	44.89	47.22	94.44
13	9	0.1	100	100	79.99	80.02	240.06
14	9	0.2	100	50	82.67	82.20	123.30
15	5	0.1	100	100	56.90	57.71	173.13
16	5	0.2	100	100	63.67	61.20	91.80
17	5	0.2	100	50	60.34	59.61	89.41
18	5	0.2	150	50	61.72	60.12	90.18
19	7	0.05	125	75	63.98	62.82	376.92
20	7	0.25	125	75	75.48	79.25	95.10
21	7	0.15	125	75	74.63	75.42	150.84
22	7	0.15	125	75	74.63	74.22	148.44
23	9	0.2	150	50	83.51	81.65	122.47
24	9	0.1	150	100	80.77	80.45	241.35
25	7	0.15	125	125	75.59	77.32	154.64
26	5	0.1	100	50	55.24	54.42	163.26
27	7	0.15	125	75	74.63	72.22	144.37
28	7	0.15	175	75	74.82	76.56	153.12
29	9	0.1	100	50	78.30	78.57	235.71
30	7	0.15	125	75	74.63	76.22	152.44

the statistical model. Actual values were close to the predicted ones. The predicted values showed a good fit and acceptable relationship compared with the actual values. In addition, the ammonium adsorption efficiency and the capacity of M/HNC for 30 runs were investigated. It is concluded that the maximum adsorption efficiency (90.04%) and adsorption capacity (376.92 mg/g) were obtained at runs 8 and 19.

The quadratic model was suggested for the description of the ammonium adsorption process by the adsorbent. According to the results, the R^2 value was close to 1 (0.98), which showed that the model was appropriate for the ammonium adsorption process. Also, the predicted R^2 (0.91) was in agreement with the adjusted R^2 (0.96), and their difference was less than 0.2. Adeq. Precision calculates the signal to noise ratio, and a ratio of more than 4 is considered ideal. In the present study, the signal to noise ratio for ammonium adsorption was 32.25, which indicated an adequate signal.

Based on the results of the ANOVA test, F_{value} (62.56) and $P_{value} < 0.05$ (for the model) showed that the model was significant for the adsorption of ammonium. The results showed that *A*, *B*, *D*, A^2, and B^2 were the significant terms of the ammonium adsorption model (*p*-value < 0.1). *F*-value (2.46) and *P*-value > 0.05 (for the lack of fit) exhibited that the lack of fit was not significant. It means that the model was fit for the ammonium adsorption process.

Furthermore, the actual equation for the quadratic model is presented by Eq. (9):

$$\begin{aligned}\text{Adsorption} = {} & -20.64305 + 12.60505\ \text{pH} + 18.31229\ \text{Adsorbent dosage} + 0.108829\ \text{Mixing speed} + 0.088846\ \text{Contact time} \\ & + 0.007350\ \text{pH} \times \text{Adsorbent dosage} \times \text{Mixing speed} + 0.000123\ \text{Mixing speed} \times \text{Contact time} - 0.456589\ \text{pH}^2 \\ & - 4.90042\ \text{Adsorbent dosage}^2 - 0.000354\ \text{Mixing speed}^2 - 0.000680\ \text{Contact time}^2 \end{aligned} \quad (9)$$

The equation in terms of coded factors demonstrated the contribution of each factor to the response. pH, adsorbent dosage, mixing speed, and contact time showed a positive contribution to the response. Also, the interactive effects of other factors were positive and negative. The equation in terms of actual factors can be applied for the prediction of response for a certain level of each factor. In this situation, the levels of each factor must be identified in the main units. This equation should not be used to determine the relative effects of each factor. In fact, the coefficients were scaled for the adjustment of units of each factor, and interception was not at the center of the design space.

3.3. Effect of different factors on the ammonium adsorption efficiency

Based on the results presented in Table 3 and Fig. 5a–f, the efficiency of ammonium adsorption from LL was increased by enhancing pH, adsorbent dosage, mixing speed, and contact time.

The pH of the solution has an important effect on the ammonium ions and surface characteristics of the adsorbents. In the present study, the effect of pH in the range of 3–11 on ammonium adsorption was investigated. Based on the observations, the efficiencies at pH 3, 5, 7, 9, and 11 were 47.22%, 54.42%–64.04%, 62.82%–79.25%, 78.57%–86.42%, and 90.04%, respectively. Variation of pH in the solution can cause the protonation and deprotonation of functional groups on the surface of clays by the adsorption of H^+ and OH^- [53]. Whenever pH increased, ammonium adsorption was also increased. In fact, negative charges are increased by increasing pH and lead to the rise of adsorption capacity [54]. It should be noted that when the value of pH increased, hydroxyl groups (OH) in the structure of montmorillonite were converted to O^- and then interacted with ammonium ions, which led to the increase of the adsorption capacity of ammonium by M/HNC [55]. However, lower efficiency in acidic conditions can be due to the presence of hydrogen ions. Hydrogen cationic ions compete with ammonium for adsorption on the surface of M/HNC [56]. Also, pH_{pzc} (pH_{pzc} = 7) showed that in the value of less than 7, the M/HNC surface had a positive charge, and in the value of more than 7, the adsorbent surface had a negative charge (Fig. 6). An increase in pH from 3 to 11 and its effects on increasing the adsorption of ammonium by chitosan-g-poly(acrylic acid)/attapulgite were reported in a study performed by Zheng et al. [57].

Adsorbent dosage is one of the most important factors in the ammonium adsorption capacity. The effect of M/HNC dosage in the range of 0.05–0.25 g/L on the adsorption of ammonium from LL was studied. Based on the results presented in Table 3 and Fig. 5a, d, and e, adsorption efficiencies for 0.05, 0.1, 0.15, 0.2, and 0.25 g/L of M/HNC were 62.86%, 54.42%–80.45%, 47.22%–90.04%, 59.61%–86.42%, and 79.25%, respectively. Increasing the adsorbent dosage from 0.05 to 0.15 g/L, increased the adsorption efficiency, which can be due to the larger surface area and availability of more adsorption sites on the adsorbent [58,59]. However, for the higher dosages of the adsorbent, the efficiencies were slightly declined. This phenomenon can be due to the equilibrium between ammonium and M/HNC in the operating condition. Also, Gupta and Bhattacharyya [21] reported that aggregation of particles in the adsorbent occurs by increasing the adsorbent dosage and leads to the reduction of surface area and subsequently, adsorption capacity. Asfaram et al. [60] reported that higher adsorbent dosages lead to interference between the adsorbate and binding sites of the adsorbent, which can cause the reduction of adsorption efficiency. Since the cost of wastewater treatment depends on the cost of the adsorbent, the optimum dosage of the adsorbent should be determined for cost-effective plans. Yang et al. [27] reported that the adsorption efficiency of ammonium was increased from 39.9% to 81.35% by increasing the adsorbent dosage (chitosan/zeolite) from 0.05 to 0.6 g. However, for the higher dosage (0.7 g), the efficiency was slightly increased (82.80%).

Agitation is another important factor in the adsorption process because the distribution of the solute in the solution media and the formation of the external boundary layer are affected by agitation [61]. The ammonium adsorption efficiencies were investigated at the mixing speed of 75–125 rpm. Based on the results presented in Table 3 and Fig. 5b, d, and f, adsorption efficiencies at 75, 100, 125, 150, and 175 rpm were 73.45%, 54.42%–85.04%, 47.22%–90.04%, 56.19%–86.42%, and 76.56%, respectively. Ammonium adsorption was increased by increasing the mixing speed (125 rpm), which can be due to the higher contact of M/HNC with ammonium [62]. However, at 175 rpm, the efficiency slightly decreased. The kinetic energy of the adsorbent particles and adsorbate ions is increased by increasing the agitation speed and results in a quick collision between them. In this situation, loosely-bound adsorbent particles are separated, and consequently, the efficiency decreases [63]. Application of granular feldspar and cockle shells for the adsorption of ammonium from LL showed that the efficiency was increased by increasing the mixing speed (40–150 rpm) and at higher mixing speeds (150–200 rpm), the efficiency was slightly decreased [64]. Also, Aziz et al. [65] investigated the adsorption of ammonium from LL by polyaluminium chloride. They reported that the efficiency was increased by increasing the mixing speed (75–150 rpm), and at the mixing speeds of 150–300 rpm, the efficiency was decreased.

The adsorption process consists of three steps: (i) movement of the pollutants to the boundary layer; (ii) diffusion of the pollutants into the surface of the adsorbent; and (iii) diffusion of the particles into the porous structure of the adsorbent. Therefore, all the steps need contact time [61]. The effect of contact time (25–125 min) on the adsorption of ammonium from LL was also studied. Based on the results presented in Table 3 and Fig. 5c, e, and f, adsorption efficiency was obtained to be 71.15%, 54.42%–82.20%, 47.22%–90.04%, 57.12%–86.42%, and 77.32% at 25, 50, 75, 100, and 125 min, respectively. The efficiency was increased by enhancing the contact time until 75 min, but after that, it was reduced. The pollutant adsorption capacity was high in the first few time intervals due to the existence of more adsorption sites at these times. This phenomenon led to more interactions between the pollutants and the adsorption sites [66]. Huang et al. [67] reported that the ammonium adsorption efficiency of zeolite and modified zeolite was increased by increasing the time (60 min), and after

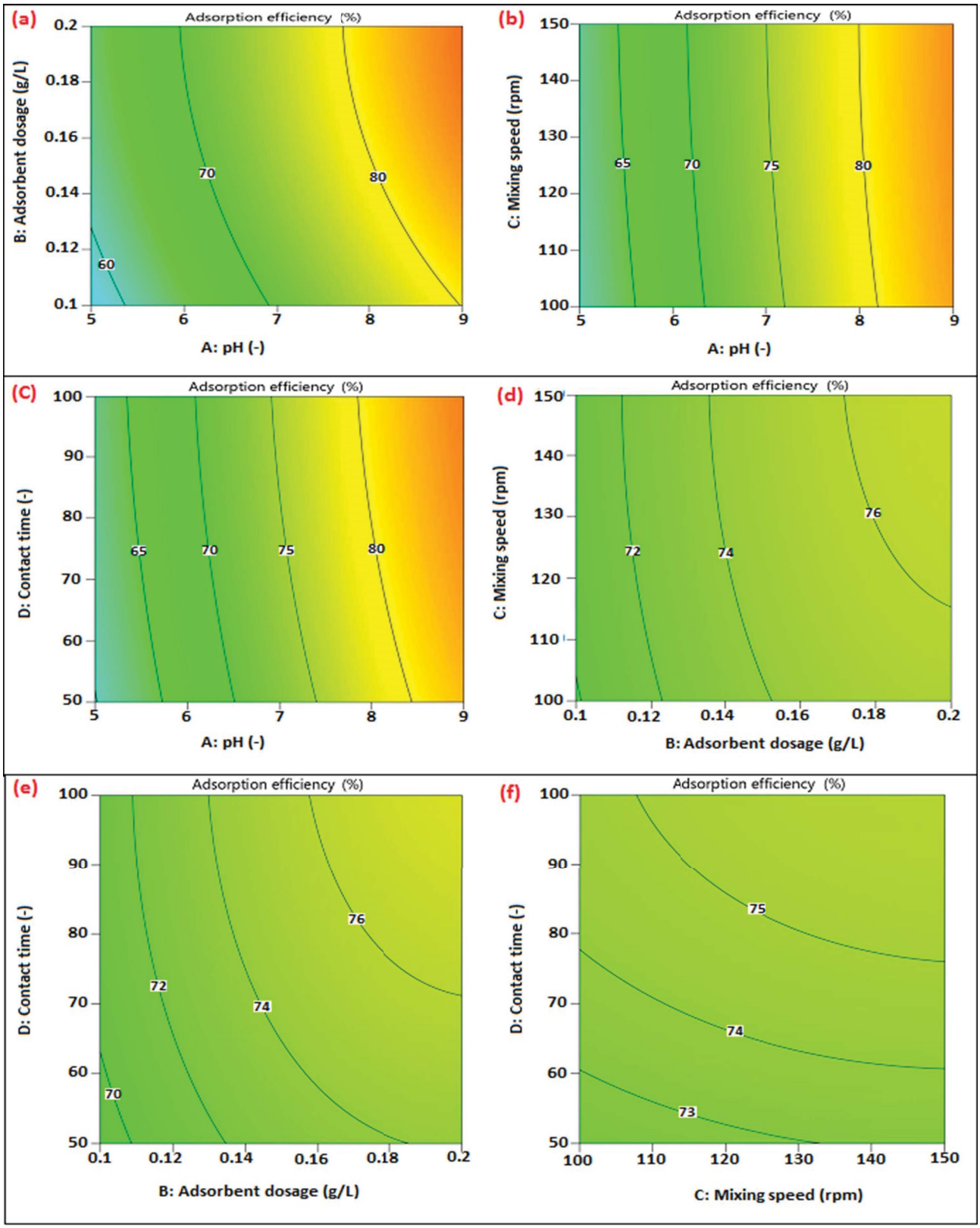

Fig. 5. The 3D graphs and the interactive effects of the considered factors on the ammonium adsorption efficiency; (a) pH and adsorbent dosage (AB), (b) pH and mixing speed (AC), (c) pH and contact time (AD), (d) adsorbent dosage and mixing speed (BC), (e) adsorbent dosage and contact time (BD), and (f) mixing speed and contact time (CD).

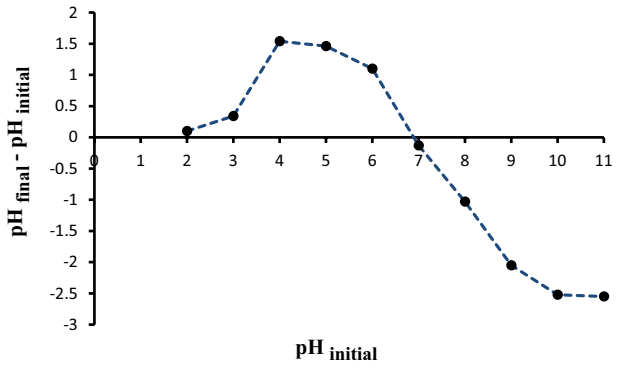

Fig. 6. pH of point of zero charge (pH_{pzc}) for M/HNC by the pH drift method.

that, the efficiency was increased slowly and reached a fixed level. Also, in another study performed by Huang et al. [68], the ammonium adsorption efficiency of Chinese zeolite was increased by increasing the contact time. The lower adsorption of ammonium on M/HNC in the next time interval (after 75 min) was due to the slower diffusion of the solute into the internal sites of the adsorbent [66]. Moreover, the large surface area of hematite was effective in the adsorption and transmission of the pollutants onto the surface of the adsorbent [69]. The most important advantage of the CCD method was examining the interactive effects of the factors on the adsorption efficiency. As shown in Fig. 5a–f, the interactions of AC, AB, AD, and BD had an increasing effect on efficiency. However, for BC and CD, the increasing effects were small. It should be noted that the addition of Fe to increase ammonia adsorption is not a novel approach, but the addition of industrial waste containing iron compounds instead of pure commercial iron compounds for modifying clays has not been investigated in another research. The main purpose of applying this iron compound (the waste from the Midrex process) was the management of industrial wastes in factories and industrial sites. If industrial wastes are reused for other applications (e.g., wastewater treatment), the amount of wastes as well as the cost of waste disposal and wastewater treatment can be reduced. In this situation, the consumption of wastes in other applications is posed as a cost-beneficial approach. Thus, it can be concluded that the M/HNC adsorbent not only can be applied in wastewater treatment but also can be utilized to reduce and manage the industrial waste of the Midrex process.

3.4. Adsorption kinetics

The obtained experimental results were modeled using pseudo-first-order and pseudo-second-order kinetic models to describe the control mechanism of ammonium adsorption on M/HNC. The graphs of pseudo-first-order (a) and pseudo-second-order (b) kinetic models at ammonium concentration of 30 mg/L over a period of 115 min are shown in Fig. 7. Table 4 summarizes the pseudo-first-order and pseudo-second-order kinetic models with their corresponding correlation coefficients (R^2) for ammonium adsorption on M/HNC at the initial ammonium concentration of 30 mg/L. It can be seen that the correlation coefficients (R^2) of the pseudo-first-order and pseudo-second-order models were 0.97 and 0.99, respectively. This indicates the suitable fit of the pseudo-second-order model compared with the pseudo-first-order model.

Numerous studies have investigated kinetic models of ammonium adsorption on different adsorbents such as Fe_3O_4 nanoparticles, modified Ca-bentonites, metakaolin geopolymer, and activated carbon/zeolite composite and they have reported that the kinetics data followed the pseudo-second-order model [10,16,26,70].

3.5. Adsorption isotherms

In the process of ammonium adsorption on M/HNC, Langmuir and Freundlich isotherm models were studied at the initial ammonium concentration of 5–30 mg/L, contact time of 0–115 min, adsorbent dose of 0.167 g/L, pH = 8.05, mixing speed of 117.42 rpm, and temperature of 25°C. Based on the results presented in Table 5 by comparing the obtained R^2 values, the conformity of ammonium adsorption with the Langmuir model (R^2 = 0.96) was better than the Freundlich model (R^2 = 0.75). This was also evident in the diagram plotted in Fig. 8 to determine the Langmuir (a) and Freundlich (b) isotherm parameters. Therefore, it can be said that ammonium adsorption on M/HNC was a monolayer and uniform (homogeneous) process with the same energy on the entire surface of the adsorbent. The K_F and n values in the Freundlich model were determined by plotting the graph of $\log(q_e)$ vs. $\log(C_e)$ (Fig. 8b). In general, in the Freundlich model, if n is equal to 5, the adsorption process is linear; if n is less than 1, the adsorption process is a chemical process, and if n is greater than 1, the absorption is a desirable physical process. Accordingly, given that the n value was obtained above 3 (Table 5), a desirable physical process occurred. However, the low correlation coefficient (R^2 = 0.75) indicated that the Freundlich model was not the best model to describe the adsorption process. Similar results have been reported for several adsorbents for ammonium adsorption isotherms. Langmuir isotherm was also the best fit model for Fe_3O_4 nanoparticle, modified Ca-bentonite, vermiculite, and natural expanded vermiculite adsorbents [10,16,17,26].

3.6. Adsorption mechanism

When montmorillonite sheets are broken, two different surfaces are created; one is resulted from the easy cleavage of the layers, is known as the "face", is composed of completely compensated oxygen atoms, shows low electrical charge, is hydrophobic, and exhibits nonpolar properties in water. The other surface is the result of the break of the ionic bonds within the layers, is named the "edge", is made up of hydroxyl ions, siloxane groups (–Si–O–Si–), O^{2-}, and Mg ions that simply undergo hydrolysis, has a comparatively high-level electrical charge, and is polar in water. The hydrophilic effect resulted from some functional hydroxyl groups such as SiOH and –MgOH on the edge surfaces [71]. The faces and the edges of the clay particles can adsorb polar pollutants as well as some anions and cations from water. The pollutants adsorb on the clay surface, which results in their immobilization due to the processes of coordination, ion exchange, or interaction between ion and dipole. The contaminants can be

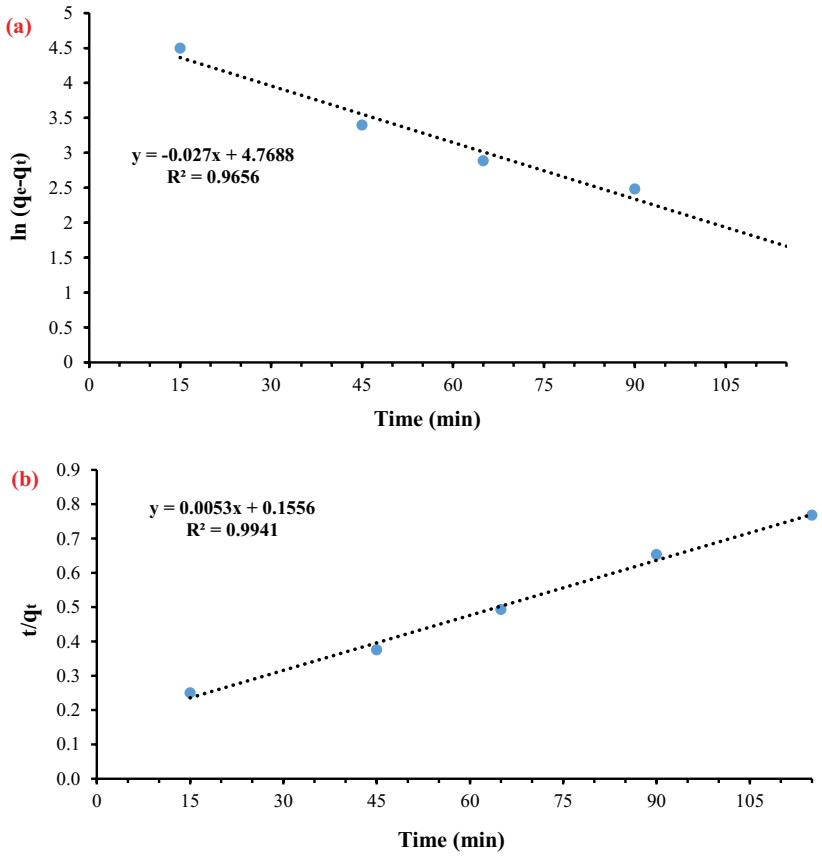

Fig. 7. Investigating the pseudo-first-order (a) and pseudo-second-order (b) kinetic models for ammonium adsorption on M/HNC (initial ammonium concentration of 30 mg/L; contact time of 0–115 min; adsorbent dose of 0.167 g/L; pH = 8.05; mixing speed of 117.42 rpm; temperature of 25°C).

held by H–bonding or Van der Waals interactions resulting from either strong or weak interactions. The strength of the interactions is determined by numerous structural properties and other features of the clay mineral [72]. According to the basic 2:1 structure, montmorillonite has a high surface charge due to the spread of isomorphous substitution in octahedral and tetrahedral sheets [21]. Two main reaction mechanisms have been reported for the ammonium adsorption process on montmorillonite. One of these mechanisms is ion exchange, which is mainly of electrostatic nature, on the permanent negatively charged sites (the siloxane groups) by forming an outer-sphere complex and another complexation on the edge sites (hydroxyl groups) by forming an inner-sphere complex which is mainly of chemical nature. Mazloomi and Jalali [73] stated that the adsorption of ammonium occurs through Na, K, Mg, and Ca ion exchange with ammonium. Thus, ammonium can be exchanged with Mg and Na in the structure of montmorillonite. Due to the interfaces between the aqueous solution and the mineral, surface complexation is a macroscopic adsorption behavior. The hydrophilic negative surface sites of montmorillonite (SiO^-) have been investigated by adsorption of cationic ions used as molecular probes. The electrostatic attraction between the opposite charge of ammonium and negative surface sites on montmorillonite leads to adsorption and suggests a strong affinity. Ammonium can be bonded to the edge surfaces of montmorillonite sheets by hydrogen bonding. Montmorillonite removes ammonium mainly by cation exchange, and the subsidiary magnetic nanoparticles possess high surface area, which

Table 4
Constants of pseudo-first-order and pseudo-second-order kinetic models for ammonium adsorption on M/HNC

Pseudo-first-order	q_e (mg/g)	k_1 (1/min)	R^2
	117.78	0.0270	0.97
Pseudo-second-order	q_e (mg/g)	k_2 (g/mg min)	R^2
	188.68	0.00018	0.99

Table 5
Constants of Langmuir and Freundlich isotherm models for ammonium adsorption on M/HNC

Langmuir			Freundlich		
R^2	q_{max} (mg/g)	K_L (L/mg)	R^2	K_F ((mg/g) (mg/L)^n)	n
0.96	5.181	1.497	0.75	4.398	6.373

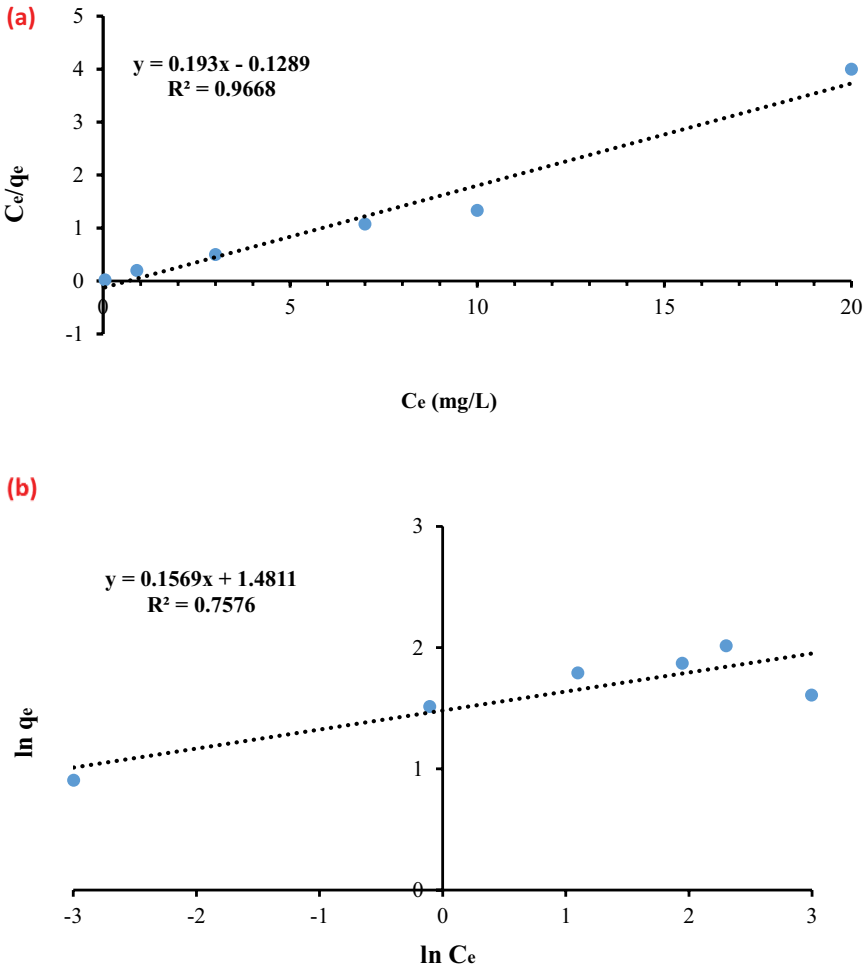

Fig. 8. Investigating Langmuir (a) and Freundlich (b) isotherm models for ammonium adsorption on M/HNC (initial ammonium concentration of 5–30 mg/L; contact time of 0–115 min; adsorbent dose of 0.167 g/L; pH = 8.05; mixing speed of 117.42 rpm; temperature of 25°C).

results in enhanced ammonium adsorption. This shows that most of the adsorption active sites of the nanoparticles can be found on the exterior of the adsorbent and are easily accessible by the ammonium ions, thus resulting in rapid adsorption [74]. Cationic pollutants such as ammonium can be adsorbed at FeO^- sites of hematite via electrostatic attraction [75]. Hematite is resistant to corrosion, is the most stable iron oxide [76], and its application can be a good option for treating acidic wastewater such as LL (shown in Table 1). Therefore, based on the mentioned mechanisms, both montmorillonite and hematite could play great roles in the synergistic ammonium adsorption effect. It is well known that electrostatic attraction and coordination between ammonium and the adsorbent is the mechanism of adsorption. In this research, the potential of hematite nanomagnetic plays an important role.

3.7. Optimization

One of the most important aims of this study was to find the optimum parameters in order to increase the response using the proposed mathematical model. As shown in Table 6, pH (8.05), M/HNC dosage (0.167 g/L), mixing speed (117.42 rpm), and contact time (81.99 min) were determined as optimum factors based on the CCD method by software. The predicted and actual adsorption efficiencies were 83% and 80%, respectively. It was demonstrated that the actual and predicted efficiencies were

Table 6
Optimum factors determined by the CCD method

	pH	Adsorbent dosage (g/L)	Mixing speed (rpm)	Contact time (min)	Adsorption efficiency (%)
Predicted by software	8.05	0.167	117.42	81.99	83
Actual leachate sample	8.05	0.167	117.42	81.99	80

close to each other. The reported adsorption efficiency for actual conditions (Table 6) was obtained after three repetitions and was based on the average with a standard deviation of 0.08 to 0.87.

3.8. Comparing the adsorption capacity of M/HNC with other adsorbents

The maximum adsorption capacity of M/HNC for the adsorption of ammonium was compared with that of other adsorbents (Table 7). As can be observed, the capacity of the M/HNC for the adsorption of ammonium is better than other adsorbents, which can be attributed to its nanostructure and surface properties. Therefore, M/HNC can be used as an effective adsorbent for the adsorption of ammonium from wastewater and aqueous solution. Moreover, the present study has some important advantages and disadvantages. The main advantage of this study is the cheaper cost of the components used for the synthesis of the M/HNC adsorbent in comparison with the cost of the components of other adsorbents. Iron waste from the Midrex process should be disposed of in the factory, but by the application of this compound in the synthesis of the adsorbent, the cost of waste management can be reduced. However, the

Table 7
Comparison of the adsorption capacity of different adsorbents and M/HNC

Adsorbents	Initial concentration of ammonium (mg/L)	pH	Maximum absorption capacity (q_{max}) (mg/g)	Reference
Pretreated Bulgarian clinoptilolite	175	6	18.40	[77]
NaCl-activated zeolite	60	7	5.92	[78]
Zeolite 13X	80	5.23	8.61	[79]
Natural Turkish (Yıldızeli) zeolite	60	8	9.64	[80]
Chitosan-g-poly(acrylic acid)/rectorite hydrogel composite	100	7	40.90	[81]
Zeolite synthesized from fly ash	100	8	24.30	[82]
Chitosan-g-poly(acrylic acid)/attapulgite composite	100	7	20.30	[57]
Boston ivy leaf powder	100	7	6.59	[83]
Sawdust	50	6	1.70	[84]
NaA zeolite/chitosan porous hybrid beads	100	6	47.62	[27]
Natural Turkish (Resadiye) bentonite	60	7	30.12	[85]
Modified Ca-bentonite	5	7	46.90	[10]
M/HNC	30	7	376.92	This study

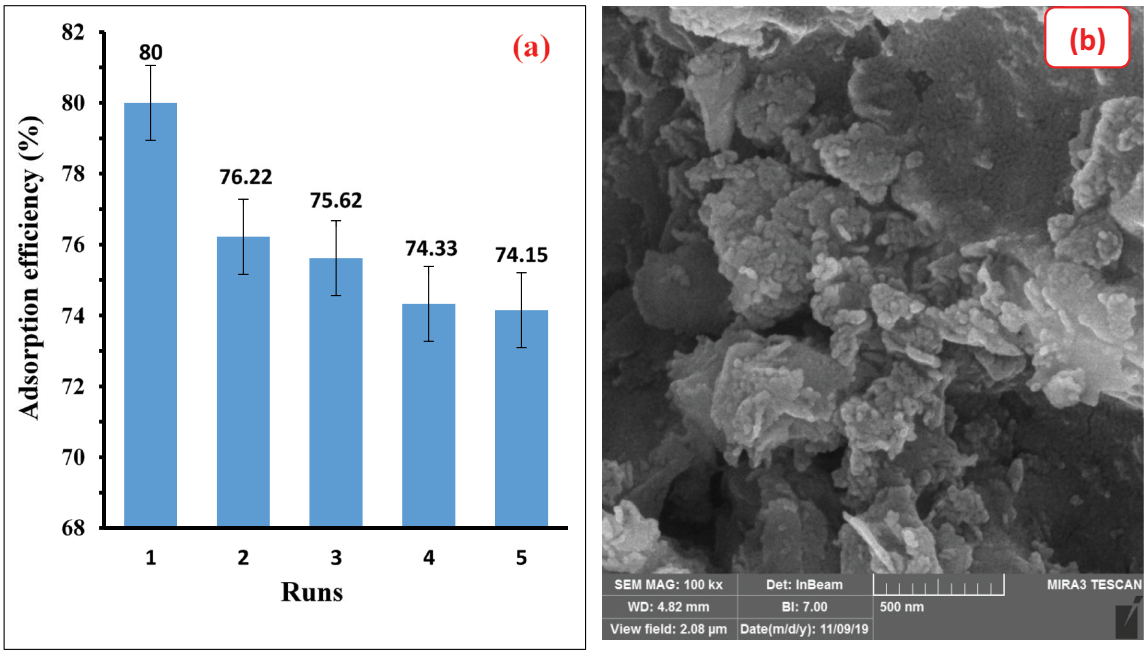

Fig. 9. Recycling and reuse of M/HNC for ammonium adsorption (pH = 8.05; initial concentration of 30 mg/L; the adsorbent dosage of 0.167 g/L; mixing speed of 117.42 rpm; contact time of 81.99 min) (a) M/HNC after five recycling cycles and (b) the SEM image.

application of adsorbents for wastewater treatment especially high-load wastewater such as LL needs a high amount of adsorbents. As mentioned earlier, LL was diluted for the experiments that can consume plenty of water and increase the volume of wastewater.

3.9. Absorbent reuse and stability

Due to the importance of adsorbent reuse, the adsorption efficiency of the recycled M/HNC for ammonium adsorption was studied. M/HNC was first separated by an external magnet and then washed with distilled water and ethanol and dried at 100°C [86]. The recycled M/HNC was added to the new ammonium solution in each run. The results showed that the adsorption efficiency of M/HNC decreased by almost 4% in the second run; however, it had relative stability in the subsequent runs, so the ammonium adsorption efficiency of the recycled M/HNC was obtained to be 74.15% in the fifth run (Fig. 9a). Then the SEM technique was employed to evaluate the chemical stability of the adsorbent after the fifth run (Fig. 9b). According to the results of SEM, it was observed that the morphological characteristics of the adsorbent were still retained after the fifth run.

4. Conclusion

In this study, ammonium adsorption was investigated under the influence of various parameters such as pH, adsorbent dosage, mixing speed, and contact time. Experimental design and analysis of the results were performed using CCD. Significant factors in each experimental design response were identified by ANOVA. The quadratic model was the most suitable model. The model fit was assessed by calculating the R^2 value. The R^2 was equal to 0.98, indicating that 98% of the variation in the response can be explained by the model. The predicted values obtained using the CCD method were in agreement with the actual values. M/HNC was synthesized with a particle size of about 26 nm (nanometer scale), magnetic properties, and a high specific surface area. Based on the results, ammonium adsorption was affected by the determined factors, and increased by increasing pH, adsorbent dosage, mixing speed, and contact time. The maximum adsorption efficiency (90.04%) was observed at pH = 11, M/HNC concentration of 0.15 g/L, mixing speed of 125 rpm, and contact time of 75 min. But, adsorption efficiency of 80% was observed at optimal conditions. The ammonium adsorption process by M/HNC was consistent with the pseudo-second-order model and was controlled by chemical reactions. The isotherm data fit well with the Langmuir isotherm and showed monolayer adsorption. The recycled M/HNC showed high adsorption efficiency and chemical stability after five runs. Therefore, based on the results of this study, it can be concluded that M/HNC has a great potential for ammonium adsorption.

Acknowledgement

This article was extracted from project NO. 15614, which was in accordance with the ethical principles and the national norms and standards for conducting medical research in Iran (approval ID: IR.SUMS.REC.1397.765) and was supported by Shiraz University of Medical Sciences.

References

[1] M.S. Hossain, A. Santhanam, N.A.N. Norulaini, A.K.M. Omar, Clinical solid waste management practices and its impact on human health and environment—a review, Waste Manage., 31 (2011) 754–766.
[2] L. Giusti, A review of waste management practices and their impact on human health, Waste Manage., 29 (2009) 2227–2239.
[3] P. Alam, K. Ahmade, Impact of solid waste on health and the environment, Int. J. Sustain. Dev. Green Econ., 2 (2013) 165–168.
[4] M. Rama, T. Laiho, O. Eklund, J. Wärnå, An evaluation of the capability of nanomodified vermiculite to in situ ammonium removal from landfill leachate, Environ. Technol. Innovation, 14 (2019) 100340, doi: 10.1016/j.eti.2019.100340.
[5] N.S.B.A. Rahman, N.A. Kamal, Removal of pollutants from landfill leachate using physicochemical technique, Int. J. Civ. Eng., 17 (2019) 1363–1371.
[6] H. Hashemi, A. Ebrahimi, A. Khodabakhshi, Investigation of anaerobic biodegradability of real compost leachate emphasis on biogas harvesting, Int. J. Environ. Sci. Technol., 12 (2015) 2841–2846.
[7] F.N. Ahmed, C.Q. Lan, Treatment of landfill leachate using membrane bioreactors: a review, Desalination, 287 (2012) 41–54.
[8] H. Hashemi, M. Hoseini, A.A. Ebrahimi, Flat sheet membrane sequencing batch bioreactor for the removal of coliforms and heavy metals from stabilized composting leachate, J. Environ. Eng., 144 (2018) 4018015, doi: 10.1061/(ASCE)EE.1943-7870.0001339.
[9] H. Eslami, H. Hashemi, R.A. Fallahzadeh, R. Khosravi, R.F. Fard, A.A. Ebrahimi, Effect of organic loading rates on biogas production and anaerobic biodegradation of composting leachate in the anaerobic series bioreactors, Ecol. Eng., 110 (2018) 165–171.
[10] Z. Sun, X. Qu, G. Wang, S. Zheng, R.L. Frost, Removal characteristics of ammonium nitrogen from wastewater by modified Ca-bentonites, Appl. Clay Sci., 107 (2015) 46–51.
[11] H. Hashemi, A. Ebrahimi, M. Mokhtari, T. Jasemizad, Removal of PAHs and heavy metals in composting leachate using the anaerobic migrating blanket reactor (AMBR) process, Desal. Water Treat., 57 (2016) 24960–24969.
[12] H. Hashemi, A. Khodabakhshi, Complete treatment of compost leachate using integrated biological and membrane filtration processes, Iran. J. Chem. Chem. Eng. (English Ed.), 35 (2016) 81–87.
[13] H. Liu, Y. Dong, Y. Liu, H. Wang, Screening of novel low-cost adsorbents from agricultural residues to remove ammonia nitrogen from aqueous solution, J. Hazard. Mater., 178 (2010) 1132–1136.
[14] R.R. Karri, J.N. Sahu, V. Chimmiri, Critical review of abatement of ammonia from wastewater, J. Mol. Liq., 261 (2018) 21–31.
[15] J. Huang, N.R. Kankanamge, C. Chow, D.T. Welsh, T. Li, P.R. Teasdale, Removing ammonium from water and wastewater using cost-effective adsorbents: a review, J. Environ. Sci., 63 (2018) 174–197.
[16] T. Luukkonen, M. Sarkkinen, K. Kemppainen, J. Rämö, U. Lassi, Metakaolin geopolymer characterization and application for ammonium removal from model solutions and landfill leachate, Appl. Clay Sci., 119 (2016) 266–276.
[17] N.C. Dias, P.A. Steiner, M.C.B. Braga, Characterization and modification of a clay mineral used in adsorption tests, J. Miner. Mater. Charact. Eng., 3 (2015) 277–288.
[18] S. Sharifnia, M.A. Khadivi, T. Shojaeimehr, Y. Shavisi, Characterization, isotherm and kinetic studies for ammonium ion adsorption by light expanded clay aggregate (LECA), J. Saudi Chem. Soc., 20 (2016) 342–351.
[19] J. Chang, J. Ma, Q. Ma, D. Zhang, N. Qiao, M. Hu, H. Ma, Adsorption of methylene blue onto Fe_3O_4/activated

montmorillonite nanocomposite, Appl. Clay Sci., 119 (2016) 132–140.
[20] B. Ma, S. Oh, W.S. Shin, S.J. Choi, Removal of Co^{2+}, Sr^{2+} and Cs^{+} from aqueous solution by phosphate-modified montmorillonite (PMM), Desalination, 276 (2011) 336–346.
[21] S.S. Gupta, K.G. Bhattacharyya, Immobilization of Pb(II), Cd(II) and Ni(II) ions on kaolinite and montmorillonite surfaces from aqueous medium, J. Environ. Manage., 87 (2008) 46–58.
[22] S.H. Lin, R.S. Juang, Heavy metal removal from water by sorption using surfactant-modified montmorillonite, J. Hazard. Mater., 92 (2002) 315–326.
[23] C.O. Ijagbemi, M.H. Baek, D.S. Kim, Montmorillonite surface properties and sorption characteristics for heavy metal removal from aqueous solutions, J. Hazard. Mater., 166 (2009) 538–546.
[24] A. Shams, F. Moazeni, Modeling and simulation of the Midrex shaft furnace: reduction, transition and cooling Zones, JOM, 67 (2015) 2681–2689.
[25] K.G. Akpomie, F.A. Dawodu, Montmorillonite-rice husk composite for heavy metal sequestration from binary aqua media: a novel adsorbent, Trans. R. Soc. S. Afr., 70 (2015) 83–88.
[26] K. Zare, H. Sadegh, R.S. Ghoshekandi, M. Asif, I. Tyagi, S. Agarwal, V.K. Gupta, Equilibrium and kinetic study of ammonium ion adsorption by Fe_3O_4 nanoparticles from aqueous solutions, J. Mol. Liq., 213 (2016) 345–350.
[27] K. Yang, X. Zhang, C. Chao, B. Zhang, J. Liu, In-situ preparation of NaA zeolite/chitosan porous hybrid beads for removal of ammonium from aqueous solution, Carbohydr. Polym., 107 (2014) 103–109.
[28] A.A. Halim, H.A. Aziz, M.A.M. Johari, K.S. Ariffin, Comparison study of ammonia and COD adsorption on zeolite, activated carbon and composite materials in landfill leachate treatment, Desalination, 262 (2010) 31–35.
[29] T.H. Martins, T.S.O. Souza, E. Foresti, Ammonium removal from landfill leachate by Clinoptilolite adsorption followed by bioregeneration, J. Environ. Chem. Eng., 5 (2017) 63–68.
[30] X. Zheng, J. Dou, J. Yuan, W. Qin, X. Hong, A. Ding, Removal of Cs^{+} from water and soil by ammonium-pillared montmorillonite/Fe_3O_4 composite, J. Environ. Sci., 56 (2017) 12–24.
[31] F. Barraqué, M.L. Montes, M.A. Fernández, R.C. Mercader, R.J. Candal, R.M.T. Sánchez, Synthesis and characterization of magnetic-montmorillonite and magnetic-organo-montmorillonite: surface sites involved on cobalt sorption, J. Magn. Magn. Mater., 466 (2018) 376–384.
[32] A. Lassoued, M.S. Lassoued, B. Dkhil, S. Ammar, A. Gadri, Synthesis, photoluminescence and magnetic properties of iron oxide (α-Fe_2O_3) nanoparticles through precipitation or hydrothermal methods, Physica E, 101 (2018) 212–219.
[33] M. Dehghani, M. Nozari, I. Golkari, N. Rostami, M.A. Shiri, Adsorption of mercury(II) from aqueous solutions using dried *Scrophularia striata* stems: adsorption and kinetic studies, Desal. Water Treat., 203 (2020) 279–291.
[34] M. Dehghani, M.A. Shiri, S. Shahsavani, N. Shamsedini, M. Nozari, Removal of Direct Red 81 dye from aqueous solution using neutral soil containing copper, Desal. Water Treat., 86 (2017) 213–220.
[35] Z. Maqbool, S. Hussain, T. Ahmad, H. Nadeem, M. Imran, A. Khalid, M. Abid, F.M. Laurent, Use of RSM modeling for optimizing decolorization of simulated textile wastewater by *Pseudomonas aeruginosa* strain ZM130 capable of simultaneous removal of reactive dyes and hexavalent chromium, Environ. Sci. Pollut. Res., 23 (2016) 11224–11239.
[36] E.A. Dil, M. Ghaedi, A. Asfaram, F. Mehrabi, F. Sadeghfar, Efficient adsorption of Azure B onto CNTs/Zn: ZnO@Ni_2P-NCs from aqueous solution in the presence of ultrasound wave based on multivariate optimization, J. Ind. Eng. Chem., 74 (2019) 55–62.
[37] A.H. Panahi, S.D. Ashrafi, H. Kamani, M. Khodadadi, E.C. Lima, F.K. Mostafapour, A.H. Mahvi, Removal of cephalexin from artificial wastewater by mesoporous silica materials using Box–Behnken response surface methodology, Desal. Water Treat., 159 (2019) 169–180.
[38] H. Kamani, G.H. Safari, G. Asgari, S.D. Ashrafi, Data on modeling of enzymatic elimination of direct red 81 using response surface methodology, Data Brief, 18 (2018) 80–86.
[39] E.A. Dil, M. Ghaedi, A. Asfaram, F. Mehrabi, A.A. Bazrafshan, Optimization of process parameters for determination of trace hazardous dyes from industrial wastewaters based on nanostructures materials under ultrasound energy, Ultrason. Sonochem., 40 (2018) 238–248.
[40] S. Bhattacharya, Central Composite Design for Response Surface Methodology and Its Application in Pharmacy, IntechOpen, 2021, doi: 10.5772/intechopen.95835.
[41] M. Dehghani, M. Nozari, I. Golkari, N. Rostami, M.A. Shiri, Adsorption and kinetic studies of hexavalent chromium by dehydrated *Scrophularia striata* stems from aqueous solutions, Desal. Water Treat., 125 (2018) 81–92.
[42] M. Khazaei, S. Nasseri, M.R. Ganjali, M. Khoobi, R. Nabizadeh, A.H. Mahvi, E. Gholibegloo, S. Nazmara, Modeling mercury(II) removal at ultra-low levels from aqueous solution using graphene oxide functionalized with magnetic nanoparticles: optimization, kinetics, and isotherm studies., Desal. Water Treat., 83 (2017) 144–158.
[43] M. Dehghani, M. Nozari, A. Fakhraei Fard, M. Ansari Shiri, N. Shamsedini, Direct red 81 adsorption on iron filings from aqueous solutions; kinetic and isotherm studies, Environ. Technol., 40 (2019) 1705–1713.
[44] Z. Gholami, S.K. Ghadiri, M. Avazpour, M.A. Fard, N. Yousefi, S.S. Talebi, M. Khazaei, M.H. Saghi, A.H. Mahvi, Removal of phosphate from aqueous solutions using modified activated carbon prepared from agricultural waste (*Populous caspica*): optimization, kinetic, isotherm, and thermodynamic studies, Desal. Water Treat., 133 (2018) 177–190.
[45] K. Rajendran, S. Sen, Adsorptive removal of carbamazepine using biosynthesized hematite nanoparticles, Environ. Nanotechnol. Monit. Manage., 9 (2018) 122–127.
[46] J. Coates, Interpretation of Infrared Spectra, A Practical Approach, R.A. Meyers, Ed., Encyclopedia of Analytical Chemistry: Applications, Theory and Instrumentation, John Wiley & Sons Ltd, Chichester, 2006, pp. 10815–10837.
[47] A. Ahmed, Y. Chaker, E.H. Belarbi, O. Abbas, J.N. Chotard, H.B. Abassi, A.N.V. Nhien, M. El Hadri, S. Bresson, XRD and ATR/FTIR investigations of various montmorillonite clays modified by monocationic and dicationic imidazolium ionic liquids, J. Mol. Struct., 1173 (2018) 653–664.
[48] D.E. Fouad, C. Zhang, H. El-Didamony, L. Yingnan, T.D. Mekuria, A.H. Shah, Improved size, morphology and crystallinity of hematite (α-Fe_2O_3) nanoparticles synthesized via the precipitation route using ferric sulfate precursor, Results Phys., 12 (2019) 1253–1261.
[49] B.A. Fil, C. Özmetin, M. Korkmaz, Characterization and electrokinetic properties of montmorillonite, Bulg. Chem. Commun., 46 (2014) 258–263.
[50] A. Kalam, A.G. Al-Sehemi, M. Assiri, G. Du, T. Ahmad, I. Ahmad, M. Pannipara, Modified solvothermal synthesis of cobalt ferrite ($CoFe_2O_4$) magnetic nanoparticles photocatalysts for degradation of methylene blue with H_2O_2/visible light, Results Phys., 8 (2018) 1046–1053.
[51] R. Wahab, F. Khan, A.A. Al-Khedhairy, Hematite iron oxide nanoparticles: apoptosis of myoblast cancer cells and their arithmetical assessment, RSC Adv., 8 (2018) 24750–24759.
[52] R. Zahedsheijani, H. Gholamiyan, A. Tarmian, H. Yousefi, Mass transfer in medium density fiberboard (MDF) modified by Na^{+} montmorillonite (Na^{+} MMT) nanoclay, Maderas, Cienc. Tecnol., 13 (2011) 163–172.
[53] M. Roosta, M. Ghaedi, A. Asfaram, Simultaneous ultrasonic-assisted removal of malachite green and safranin O by copper nanowires loaded on activated carbon: central composite design optimization, RSC Adv., 5 (2015) 57021–57029.
[54] M. Zhao, Z. Tang, P. Liu, Removal of methylene blue from aqueous solution with silica nano-sheets derived from vermiculite, J. Hazard. Mater., 158 (2008) 43–51.
[55] C. Feng, S. Zhang, Y. Wang, G. Wang, X. Pan, Q. Zhong, X. Xu, L. Luo, L. Long, P. Yao, Synchronous removal of ammonium and phosphate from swine wastewater by two agricultural waste

based adsorbents: performance and mechanisms, Bioresour. Technol., 307 (2020) 123231, doi: 10.1016/j.biortech.2020.123231.
[56] K.G. Bhattacharyya, S.S. Gupta, Kaolinite, montmorillonite, and their modified derivatives as adsorbents for removal of Cu(II) from aqueous solution, Sep. Purif. Technol., 50 (2006) 388–397.
[57] Y. Zheng, J. Zhang, A. Wang, Fast removal of ammonium nitrogen from aqueous solution using chitosan-g-poly(acrylic acid)/attapulgite composite, Chem. Eng. J., 155 (2009) 215–222.
[58] R. Abbassi, A.K. Yadav, N. Kumar, S. Huang, P.R. Jaffe, Modeling and optimization of dye removal using "green" clay supported iron nano-particles, Ecol. Eng., 61 (2013) 366–370.
[59] G.K. Sarma, S.S. Gupta, K.G. Bhattacharyya, RETRACTED: Adsorption of Crystal violet on raw and acid-treated montmorillonite, K10, in aqueous suspension, 171 (2016) 1–10.
[60] A. Asfaram, M. Ghaedi, H. Abidi, H. Javadian, M. Zoladl, F. Sadeghfar, Synthesis of Fe_3O_4@CuS@Ni_2P-CNTs magnetic nanocomposite for sonochemical-assisted sorption and preconcentration of trace Allura Red from aqueous samples prior to HPLC-UV detection: CCD-RSM design, Ultrason. Sonochem., 44 (2018) 240–250.
[61] M. Khodaie, N. Ghasemi, B. Moradi, M. Rahimi, Removal of methylene blue from wastewater by adsorption onto $ZnCl_2$ activated corn husk carbon equilibrium studies, J. Chem., 2013 (2013), doi: 10.1155/2013/383985.
[62] A.R. Tembhurkar, R. Deshpande, Powdered activated lemon peels as adsorbent for removal of cutting oil from wastewater, J. Hazard. Toxic Radioact. Waste, 16 (2012) 311–315.
[63] K. Kuśmierek, A. Świątkowski, The influence of different agitation techniques on the adsorption kinetics of 4-chlorophenol on granular activated carbon, React. Kinet. Mech. Catal., 116 (2015) 261–271.
[64] Z. Daud, M.H. Abubakar, A.A. Abdul Latiff, H. Awang, Z. Ahmad, M.B. Ridzuan, COD and ammonia removal from landfill leachate using mixed granular absorbent media, J. Teknol. (Sciences Eng.), 80 (2018) 81–86.
[65] H.A. Aziz, Z. Daud, M.N. Adlan, Y.T. Hung, The use of polyaluminium chloride for removing colour, COD and ammonia from semi-aerobic leachate, Int. J. Environ. Eng., 1 (2009) 20–35.
[66] P. Wu, W. Wu, S. Li, N. Xing, N. Zhu, P. Li, J. Wu, C. Yang, Z. Dang, Removal of Cd^{2+} from aqueous solution by adsorption using Fe-montmorillonite, J. Hazard. Mater., 169 (2009) 824–830.
[67] H. Huang, D. Xiao, R. Pang, C. Han, L. Ding, Simultaneous removal of nutrients from simulated swine wastewater by adsorption of modified zeolite combined with struvite crystallization, Chem. Eng. J., 256 (2014) 431–438.
[68] H. Huang, X. Xiao, B. Yan, L. Yang, Ammonium removal from aqueous solutions by using natural Chinese (Chende) zeolite as adsorbent, J. Hazard. Mater., 175 (2010) 247–252.
[69] C.Y. Cao, J. Qu, W.S. Yan, J.F. Zhu, Z.Y. Wu, W.G. Song, Low-cost synthesis of flowerlike α-Fe_2O_3 nanostructures for heavy metal ion removal: adsorption property and mechanism, Langmuir, 28 (2012) 4573–4579.
[70] R. Malekian, J.A. Koupai, S.S. Eslamian, S.F. Mousavi, K.C. Abbaspour, M. Afyuni, Ion-exchange process for ammonium removal and release using natural Iranian zeolite, Appl. Clay Sci., 51 (2011) 323–329.
[71] M. Sprynskyy, T. Kowalkowski, H. Tutu, E.M. Cukrowska, B. Buszewski, Adsorption performance of talc for uranium removal from aqueous solution, Chem. Eng. J., 171 (2011) 1185–1193.
[72] K.G. Bhattacharyya, S.S. Gupta, Adsorption of a few heavy metals on natural and modified kaolinite and montmorillonite: a review, Adv. Colloid Interface Sci., 140 (2008) 114–131.
[73] F. Mazloomi, M. Jalali, Adsorption of ammonium from simulated wastewater by montmorillonite nanoclay and natural vermiculite: experimental study and simulation, Environ. Monit. Assess., 189 (2017) 1–19.
[74] K. Kalantari, M.B. Ahmad, H.R.F. Masoumi, K. Shameli, M. Basri, R. Khandanlou, Rapid and high capacity adsorption of heavy metals by Fe_3O_4/montmorillonite nanocomposite using response surface methodology: preparation, characterization, optimization, equilibrium isotherms, and adsorption kinetics study, J. Taiwan Inst. Chem. Eng., 49 (2015) 192–198.
[75] A. Sengupta, S. Mallick, D. Bahadur, Tetragonal nanostructured zirconia modified hematite mesoporous composite for efficient adsorption of toxic cations from wastewater, J. Environ. Chem. Eng., 5 (2017) 5285–5292.
[76] J. Yang, B. Hou, J. Wang, B. Tian, J. Bi, N. Wang, X. Li, X. Huang, Nanomaterials for the removal of heavy metals from wastewater, Nanomaterials, 9 (2019) 424, doi: 10.3390/nano9030424.
[77] P. Vassileva, D. Voikova, Investigation on natural and pretreated Bulgarian clinoptilolite for ammonium ions removal from aqueous solutions, J. Hazard. Mater., 170 (2009) 948–953.
[78] A. Alshameri, C. Yan, Y. Al-Ani, A.S. Dawood, A. Ibrahim, C. Zhou, H. Wang, An investigation into the adsorption removal of ammonium by salt activated Chinese (Hulaodu) natural zeolite: kinetics, isotherms, and thermodynamics, J. Taiwan Inst. Chem. Eng., 45 (2014) 554–564.
[79] H. Zheng, L. Han, H. Ma, Y. Zheng, H. Zhang, D. Liu, S. Liang, Adsorption characteristics of ammonium ion by zeolite 13X, J. Hazard. Mater., 158 (2008) 577–584.
[80] K. Saltalı, A. Sarı, M. Aydın, Removal of ammonium ion from aqueous solution by natural Turkish (Yıldızeli) zeolite for environmental quality, J. Hazard. Mater., 141 (2007) 258–263.
[81] Y. Zheng, A. Wang, Evaluation of ammonium removal using a chitosan-g-poly(acrylic acid)/rectorite hydrogel composite, J. Hazard. Mater., 171 (2009) 671–677.
[82] M. Zhang, H. Zhang, D. Xu, L. Han, D. Niu, B. Tian, J. Zhang, L. Zhang, W. Wu, Removal of ammonium from aqueous solutions using zeolite synthesized from fly ash by a fusion method, Desalination, 271 (2011) 111–121.
[83] H. Liu, Y. Dong, H. Wang, Y. Liu, Adsorption behavior of ammonium by a bioadsorbent – Boston ivy leaf powder, J. Environ. Sci., 22 (2010) 1513–1518.
[84] M.A. Wahab, S. Jellali, N. Jedidi, Ammonium biosorption onto sawdust: FTIR analysis, kinetics and adsorption isotherms modeling, Bioresour. Technol., 101 (2010) 5070–5075.
[85] K. Saltali, A. Sarı, Sorption capacity and thermodynamic properties of natural Turkish (Reşadiye) bentonite for the removal of ammonium ions from aqueous solution, Adsorpt. Sci. Technol., 24 (2006) 749–760.
[86] A. Nasiri, M. Malakootian, M.A. Shiri, G. Yazdanpanah, M. Nozari, $CoFe_2O_4$@methylcellulose synthesized as a new magnetic nanocomposite to tetracycline adsorption: modeling, analysis, and optimization by response surface methodology, J. Polym. Res., 28 (2021) 192.